This article has been accepted for publication in a future issue of this journal, but has not been fully edited. Content may change prior to final publication. Citation information: DOI 10.1109/LWC.2020.3046952, IEEE Wireless Communications Letters

Quantized Polar Transmitters for Power Efficient Massive MIMO Systems

Guixian Xu, Vesa Lampu, Marko Kosunen, Kari Stadius, Jussi Ryynänen, Mikko Valkama, and Lauri Anttila

***Abstract*—This letter investigates the feasibility of the quantized digital polar transmitter architecture in a downlink multi-user massive multiple-input multiple-output orthogonal frequency-division multiplexing (MIMO-OFDM) system, where a low amplitude resolution and a moderate phase resolution are utilized. We derive a lower bound on the average sum-rate achievable with Gaussian signaling inputs and linear precoding by a simple diagonal approximation for the quantization distortion. The analysis and simulations demonstrate that the quantized polar transmitter can enable excellent performance in terms of average sum-rate throughput, symbol error rate (SER), and out-of-band (OOB) emission level, thus providing an attractive option for the traditional Cartesian architecture.**

***Index Terms*—Massive MIMO, OFDM, linear precoding, transmitter architectures, polar transmitter, power efficiency, quantization.**

I. Introduction

THE practical implementation of a massive multiple-input multiple-output (MIMO) transmitter with hundreds or even thousands of antennas is a significant challenge for the future generation of cellular networks [1]. First and foremost, the cost and power consumption of the radio-frequency (RF) parts grow rapidly with the number of antennas. Furthermore, wideband orthogonal frequency-division multiplexing (OFDM) signals and complex modulation schemes utilized result in high peak-to-average power ratio (PAPR), which requires substantial backing-off of the power amplifiers (PAs), leading to poor power efficiency.

To conquer the power efficiency challenge, a well-known option is to use constant envelope (CE) waveforms, which would enable the utilization of power-efficient switching PAs. CE waveforms, however, have a spectral efficiency penalty compared to I/Q modulated waveforms. An alternative approach was proposed in [2], [3], where CE precoding was developed. Here, the constant amplitude antenna signals are generated, through optimization, from original single-carrier I/Q signals with larger PAPR, and the I/Q modulated signals are reconstructed at the receiver antennas. This approach, however, also suffers from a loss in the achievable data rate, since a large part of the transmitted power is wasted into the channel null-space. Thus [4] proposed a multi-envelope precoding scheme to alleviate this problem. However, the CE and multi-envelope precoders need to be optimized for each transmitted symbol, and thus suffer from very high complexity.

This work was supported in part by the Academy of Finland under Grants 323461, 321613, and 301820.

G. Xu, V. Lampu, M. Valkama, and L. Anttila are with the Department of Electrical Engineering, Tampere University, 33720 Tampere, Finland (e-mail: guixian.xu@tuni.fi; vesa.lampu@tuni.fi; mikko.valkama@tuni.fi; lauri.anttila@tuni.fi).

M. Kosunen, K. Stadius, and J. Ryynänen are with the Department of Electronics and Nanoengineering, School of Electrical Engineering, Aalto University, 02150 Espoo, Finland.

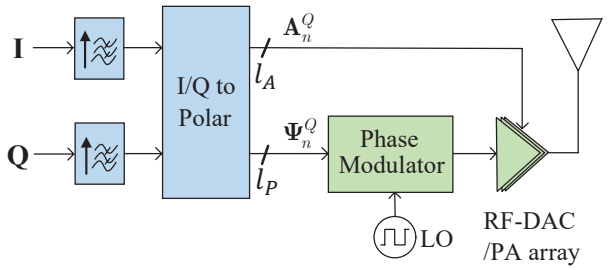

Fig. 1. Block diagram of a digital polar transmitter structure.

An appealing, though sub-optimal, alternative is to simply use linear precoding together with low-resolution digital-to-analog converters (DACs), as was proposed and analyzed in [5] in the context of the Cartesian transmitter architecture. The authors considered multi-bit DACs and linear precoding, such as maximum ratio transmission (MRT) and zero-forcing (ZF), for wideband downlink multi-user massive MIMO transmission. It was shown that the reliability performance attainable with infinite-resolution DACs can be approached with only 3-4 bit DACs, where the base station (BS) uses 128 antennas to serve 16 single-antenna users. The approach relied on the assumption that no PA is used, but the low-resolution DAC outputs are upconverted and then directly summed to form the I/Q modulated waveform. The omission of the PA severely limits the output power of the individual TXs. Addition of PAs, on the other hand, would cause a similar power efficiency challenge as regular Cartesian transmitters face, since the combined I/Q modulated signal has a high PAPR.

Alternatively, the digitally modulated polar transmitter architecture is an attractive option to the Cartesian architecture, to enable the challenging combination of wideband, power-efficient and linear operation at low cost [6]–[8]. A high-level illustration of the digital polar architecture is shown in Fig. 1. In this structure, a digital phase modulator is feeding a power-amplifying RF-DAC unit, being digitally controlled with the quantized amplitude signal [7]. This structure enables the use of highly power-efficient switching PAs or switched-capacitor PA structures. It also enables the whole transmitter to be integrated on a single chip, decreasing system cost and form-factor. In addition, the polar architecture has a power efficiency gain of up to 3 dB compared to the Cartesian, due to the omission of I/Q signal summation [9]. Moreover, a comprehensive analytical study followed by a CMOS implementation of a polar quantizer chip prototype demonstrated the

This article has been accepted for publication in a future issue of this journal, but has not been fully edited. Content may change prior to final publication. Citation information: DOI 10.1109/LWC.2020.3046952, IEEE Wireless Communications Letters

superiority of signal-to-quantization-noise ratio improvement compared to rectangular (I/Q) quantizer [10]. It also showed that the maximum quantization error of large-amplitude input signals is dominated by the phase resolution.

Thus far, the digital polar architecture has not been considered and analyzed for the design of multi-user massive MIMO transmitters. The main objective of this letter is to explore and understand the opportunities of the quantized polar transmitter in this context. Specifically, we consider a wideband downlink multi-user massive MIMO-OFDM system and focus on the case of utilizing a few amplitude bits and a moderate number of phase bits in the polar transmitter. In modern CMOS technologies, the maximum achievable amplitude resolution is decreased with continuous scaling of low supply voltage and device feature size, whereas the phase resolution is increased by the faster transition times and higher maximum oscillation frequency of nanoscale CMOS [10], [11]. Therefore, we argue that a higher number of phase bits is a feasible assumption.

With Gaussian signaling inputs and ZF precoding, we derive a lower bound on the average sum-rate throughput by a diagonal approximation method, which assumes that the distortion is uncorrelated in both the spatial and temporal domains. Finally, simulation results demonstrate the superior performance of the polar architecture in terms of average sum-rate, symbol error rate (SER), and out-of-band (OOB) emission level, compared to the Cartesian architecture.

II. System Model

We consider a single-cell downlink multi-user massive MIMO system with OFDM transmission over frequency-selective channels, where the BS is equipped with N_t antennas, simultaneously serving K single-antenna user equipments (UEs). At the BS, the frequency-domain precoded vector of data symbols is mapped to a discrete-time OFDM signal at each antenna by performing inverse discrete Fourier transform (IDFT) before being passed to the polar transmitter. We denote the subcarrier spacing by Δf and the number of subcarriers by N_{sc}. We assume oversampling with an integer factor κ through frequency-domain zero-padding. The IDFT size is then $N = \kappa N_{sc}$, and the time-domain signal has a sample interval of $T_c = \frac{1}{N\Delta f}$.

Let $\mathbf{u}_l = [u_{1,l}, \cdots, u_{K,l}]^T \in \mathcal{O}^K$ be the symbol vector associated with the l-th subcarrier ($l = 0, \cdots, N-1$), where $\mathcal{O}$ represents the quadrature amplitude modulation (QAM) alphabet. We use $\mathcal{S}_u$ to denote the set of S active subcarriers associated with intended data symbols. For the $N - S$ guard subcarriers, we assume that $u_{k,l} = 0$, and unit average power for the active subcarriers, i.e., $\mathbb{E}[\|\mathbf{u}_l\|^2] = \mathbf{I}_K$ for $l \in \mathcal{S}_u$. The transmitted time-domain signal $\mathbf{z}_n$ is generated by multiplying $\mathbf{u}_l$ with the precoding matrices $\{\mathbf{P}_l\}$, and then applying normal OFDM processing at each transmit branch. Moreover, the transmitted signal $\mathbf{z}_n$ is assumed to satisfy

$$\mathbb{E}\Big[\sum_{n=0}^{N-1} \|\mathbf{z}_n\|^2\Big] = P_{\text{total}}, \tag{1}$$

where P_{total} denotes the total transmit power at the BS. With perfect channel state information at the BS, we can rewrite $\mathbf{z}_n$ as

$$\mathbf{z}_n = \frac{1}{\sqrt{N}} \sum_{l \in \mathcal{S}_u} \mathbf{P}_l \mathbf{u}_l \exp(j\frac{2\pi}{N} ln) \tag{2}$$

for $n = 0, 1, \cdots, N-1$, where $\mathbf{P}_l = \beta \widehat{\mathbf{H}}_l^H (\widehat{\mathbf{H}}_l \widehat{\mathbf{H}}_l^H)^{-1} \in \mathbb{C}^{N_t \times K}$ is the ZF precoder associated with l-th subcarrier while power scaling constant $\beta = \sqrt{\frac{P_{\text{total}}}{\frac{1}{N}\sum_{l \in \mathcal{S}_u} \text{Tr}(\widehat{\mathbf{H}}_l \widehat{\mathbf{H}}_l^H)^{-1}}}$ is adopted to ensure that total average transmit power constraint (1) holds. The matrix $\widehat{\mathbf{H}}_l \in \mathbb{C}^{K \times N_t}$ is the frequency-domain channel matrix between the BS and UEs at the l-th subcarrier. For this, we adopt a cluster-based channel model [12] to address the frequency-selectivity and spatial correlation characteristics of the massive MIMO channels.

A. Polar Transmitter Architecture

In this work, a digital polar transmitter architecture [7], [8] is adopted at the BS, instead of the conventional and popular Cartesian architecture. Fig. 1 shows the block diagram of the digitally modulated polar transmitter, where the I/Q signal is first upsampled and pulse-shaped. Then, the I/Q signal components of the time-domain per-antenna transmitted signal are converted to a polar representation in the digital domain. After that, the amplitude and phase signals are quantized independently. Specifically, the amplitude signal directly modulates an l_A-bit resolution (e.g., $L_A = 2^{l_A}$ quantization levels) RF-DAC, acting also as the PA, while the phase signal, quantized to l_{P} bits, is passed to the digital phase modulator. The phase modulator can be realized with, for example, a digital phase-locked loop (PLL), a delay line based approach, or through I/Q modulation. In the last step, the phase modulated signal is modulated with the amplitude signal in the RF-DAC to generate the RF output signal at the desired carrier frequency. For simplicity, we assume that other RF components are ideal without impairments, and assume perfect timing between the amplitude and phase paths as well as perfect synchronization between the BS and UEs.

The amplitude and phase signals at the n-th time sample are given by

$$\mathbf{A}_n = \sqrt{\Re\{\mathbf{z}_n\}^2 + \Im\{\mathbf{z}_n\}^2}, \tag{3}$$

$$\mathbf{\Psi}_n = \arctan\left(\frac{\Im\{\mathbf{z}_n\}}{\Re\{\mathbf{z}_n\}}\right), \tag{4}$$

where the amplitude signal $\mathbf{A}_n$ follows the Rayleigh distribution, as the I/Q signal branches follow independent identically distributed zero-mean asymptotically Gaussian distributions for a sufficiently large number of subcarriers, and the phase signal $\mathbf{\Psi}_n$ follows a uniform distribution in the interval $[0, 2\pi]$.

B. Uniform Quantization

Uniform real-valued quantization is adopted in the polar transmitter for both the amplitude and phase paths. For the phase path, the 2π phase range is divided into $L_P = 2^{l_P}$, $\frac{2\pi}{L_P}$-rotationally symmetric sectors [3]. The input phase signal belonging to the p-th sector is quantized (mapped) to $\frac{(2p-1)\pi}{L_P}$. Hence, the output of the phase quantizer can be expressed as

$$\mathbf{\Psi}_n^{\text{Q}} = \left(\left\lfloor \frac{\mathbf{\Psi}_n}{2\pi/L_P} \right\rfloor + \frac{1}{2}\right) \frac{2\pi}{L_P}, n = 0, \cdots, N-1, \tag{5}$$

This article has been accepted for publication in a future issue of this journal, but has not been fully edited. Content may change prior to final publication. Citation information: DOI 10.1109/LWC.2020.3046952, IEEE Wireless Communications Letters

where the operator $\lfloor\cdot\rfloor$ denotes the floor operation.

Conversely, the amplitude quantization is more complicated due to the Rayleigh input. In general, one should choose the best step size for minimizing the quantization distortion caused by the finite amplitude resolution. However, too small a step size will result in significant overload distortion, while there will be considerable granular distortion if it is too large. Here, we set the clipping level $\mathcal{A}_{\text{clip}}$ of the amplitude quantizer such that the overload distortion power is determined by using the knowledge of the Rayleigh distribution of amplitude signal (cf. (25)). Hence, with L_A quantization levels, the step size is $\frac{\mathcal{A}_{\text{clip}}}{L_A}$ and the quantized amplitude is given by

$$\mathbf{A}_n^{\text{Q}} = \left(\left\lfloor \frac{\mathbf{A}_n}{\mathcal{A}_{\text{clip}}/L_A} \right\rfloor + \frac{1}{2}\right)\frac{\mathcal{A}_{\text{clip}}}{L_A}, n = 0, \cdots, N-1. \quad (6)$$

Finally, at each BS antenna, the quantized transmitted signal at the n-th time sample can be written as

$$\mathbf{x}_n = \mathbf{A}_n^Q \odot \exp(j\mathbf{\Psi}_n^Q), \quad (7)$$

where the operator $\odot$ denotes the Hadamard product.

The quantization error model for the amplitude and phase quantization at the n-th time sample can be written as the following generalized additive error model:

$$\mathbf{A}_n^Q = \mathbf{A}_n + \mathbf{e}_{\mathbf{A}_n}, \quad (8)$$

$$\mathbf{\Psi}_n^Q = \mathbf{\Psi}_n + \mathbf{e}_{\mathbf{\Psi}_n}. \quad (9)$$

Then, the exponential part in (7) reads $\exp(j\mathbf{\Psi}_n^Q) = \exp(j\mathbf{\Psi}_n)\exp(j\mathbf{e}_{\mathbf{\Psi}_n})$. Applying the second-order Taylor approximation to $\exp(j\mathbf{e}_{\mathbf{\Psi}_n})$ yields

$$\exp(j\mathbf{e}_{\mathbf{\Psi}_n}) \approx 1 + j\mathbf{e}_{\mathbf{\Psi}_n} - \frac{1}{2}\mathbf{e}_{\mathbf{\Psi}_n}^2. \quad (10)$$

Finally, by inserting (8), (9) and (10) into (7), we obtain the quantized transmitted signal $\mathbf{x}_n$:

$$\mathbf{x}_n \triangleq \mathbf{z}_n + \mathbf{d}_n, \quad (11)$$

and the overall quantization error can be written as $\mathbf{d}_n = \mathbf{d}_n^{(1)} + \mathbf{d}_n^{(2)}$, where $\mathbf{d}_n^{(1)} \triangleq j\mathbf{z}_n \odot \mathbf{e}_{\mathbf{\Psi}_n} + (\mathbf{e}_{\mathbf{A}_n} + j\mathbf{e}_{\mathbf{A}_n} \odot \mathbf{e}_{\mathbf{\Psi}_n}) \odot \exp(j\mathbf{\Psi}_n)$ and $\mathbf{d}_n^{(2)} \triangleq -\frac{1}{2}[\mathbf{z}_n + \mathbf{e}_{\mathbf{A}_n} \odot \exp(j\mathbf{\Psi}_n)] \odot \mathbf{e}_{\mathbf{\Psi}_n}^2$.

III. Achievable Sum-Rate Analysis

A. Achievable Sum-Rate with Gaussian Signaling

Let $\widehat{\mathbf{X}} = \mathbf{X}\mathbf{W}_N$ be transmit signal matrix in the frequency-domain, where $\mathbf{W}_N$ is the $N \times N$ DFT matrix with property that $\mathbf{W}_N\mathbf{W}_N^H = N\mathbf{I}_N$, and $\mathbf{X} = [\mathbf{x}_0, \mathbf{x}_1, \cdots, \mathbf{x}_{N-1}]$ is the corresponding time-domain transmit signal matrix over N time samples. Then, the received frequency-domain signal $\widehat{\mathbf{y}}_l \in \mathbb{C}^K$ over K UEs at the l-th subcarrier can be expressed as

$$\widehat{\mathbf{y}}_l = \widehat{\mathbf{H}}_l\widehat{\mathbf{x}}_l + \widehat{\mathbf{n}}_l, \quad (12)$$

where $\widehat{\mathbf{x}}_l$ is the l-th column of $\widehat{\mathbf{X}}$, $\widehat{\mathbf{n}}_l \sim \mathcal{CN}(\mathbf{0}, N_0\mathbf{I}_K)$ and N_0 is the noise power. Then, the transmit signal-to-noise ratio (SNR) is defined as P_{total}/N_0.

Next, we rewrite the compact form for the frequency-domain received signal over N subcarriers as

$$\widehat{\mathbf{y}} = \widehat{\mathbf{H}}\widehat{\mathbf{x}} + \widehat{\mathbf{n}}, \quad (13)$$

where $\widehat{\mathbf{y}} = \text{vec}([\widehat{\mathbf{y}}_0, \widehat{\mathbf{y}}_1, \cdots, \widehat{\mathbf{y}}_{N-1}]) \in \mathbb{C}^{KN}$ and $\widehat{\mathbf{n}} = \text{vec}([\widehat{\mathbf{n}}_0, \widehat{\mathbf{n}}_1, \cdots, \widehat{\mathbf{n}}_{N-1}]) \in \mathbb{C}^{KN}$, $\widehat{\mathbf{H}} = \text{blkdiag}([\widehat{\mathbf{H}}_0, \widehat{\mathbf{H}}_1, \cdots, \widehat{\mathbf{H}}_{N-1}]) \in \mathbb{C}^{KN \times N_t N}$, and $\widehat{\mathbf{x}} = \text{vec}(\widehat{\mathbf{X}})$ that can be expressed as

$$\widehat{\mathbf{x}} = (\mathbf{W}_N \otimes \mathbf{I}_{N_t})(\mathbf{z} + \mathbf{d}), \quad (14)$$

where the operator $\otimes$ denotes the Kronecker product, the quantization error $\mathbf{d} = \text{vec}([\mathbf{d}_0, \mathbf{d}_1, \cdots, \mathbf{d}_{N-1}]) \in \mathbb{C}^{N_t N}$, and the discrete-time precoded vector $\mathbf{z}$ is given by

$$\mathbf{z} = (\mathbf{W}_N^H \otimes \mathbf{I}_{N_t})\widehat{\mathbf{P}}\widehat{\mathbf{u}}, \quad (15)$$

wherein $\widehat{\mathbf{P}} = \text{blkdiag}([\mathbf{P}_0, \mathbf{P}_1, \cdots, \mathbf{P}_{N-1}]) \in \mathbb{C}^{N_t N \times KN}$ and $\widehat{\mathbf{u}} = \text{vec}([\mathbf{u}_0, \mathbf{u}_1, \cdots, \mathbf{u}_{N-1}]) \in \mathbb{C}^{KN}$. As a result, we can rewrite (13) as

$$\begin{aligned}\widehat{\mathbf{y}} &= \widehat{\mathbf{H}}(\mathbf{W}_N \otimes \mathbf{I}_{N_t})(\mathbf{z} + \mathbf{d}) + \widehat{\mathbf{n}} \\ &= \widehat{\mathbf{H}}(\mathbf{W}_N \otimes \mathbf{I}_{N_t})[(\mathbf{W}_N^H \otimes \mathbf{I}_{N_t})\widehat{\mathbf{P}}\widehat{\mathbf{u}} + \mathbf{d}] + \widehat{\mathbf{n}} \\ &= \widehat{\mathbf{H}}\widehat{\mathbf{P}}\widehat{\mathbf{u}} + \widehat{\mathbf{H}}(\mathbf{W}_N \otimes \mathbf{I}_{N_t})\mathbf{d} + \widehat{\mathbf{n}}. \end{aligned} \quad (16)$$

Let $\widehat{y}_{k,l} = [\widehat{\mathbf{y}}_l]_k$ be the received signal for the k-th UE at the l-th subcarrier, then we have

$$\begin{aligned}\widehat{y}_{k,l} = [\widehat{\mathbf{H}}_l\mathbf{P}_l]_{k,k}u_{k,l} + \sum_{m \neq k}[\widehat{\mathbf{H}}_l\mathbf{P}_l]_{k,m}u_{m,l} \\ + [\widehat{\mathbf{H}}(\mathbf{W}_N \otimes \mathbf{I}_{N_t})\mathbf{d}]_{k+lK,k+lK} + \widehat{n}_{k,l}, \end{aligned} \quad (17)$$

where data symbol $u_{k,l} = [\mathbf{u}_l]_k$ and noise $\widehat{n}_{k,l} = [\widehat{\mathbf{n}}_l]_k$.

With the Gaussian signaling inputs, i.e., $\mathbf{u}_l \sim \mathcal{CN}(\mathbf{0}, \mathbf{I}_K)$ for $l \in \mathcal{S}_u$, the signal-to-interference-noise-and-distortion ratio (SINDR) for UE k at the l-th subcarrier can be expressed as [5]

$$SINDR_{k,l}(\widehat{\mathbf{H}}) = \frac{|\widehat{\mathbf{H}}_l\mathbf{P}_l|_{k,k}^2}{\sum_{m \neq k}|\widehat{\mathbf{H}}_l\mathbf{P}_l|_{k,m}^2 + \Delta_{k,l}(\widehat{\mathbf{H}}) + N_0}, \quad (18)$$

where

$$\Delta_{k,l}(\widehat{\mathbf{H}}) = [\widehat{\mathbf{H}}(\mathbf{W}_N \otimes \mathbf{I}_{N_t})\mathbf{C}_{\mathbf{d}}(\mathbf{W}_N^H \otimes \mathbf{I}_{N_t})\widehat{\mathbf{H}}^H]_{k+lK,k+lK}$$

and $\mathbf{C}_{\mathbf{d}} = \mathbb{E}[\mathbf{d}\mathbf{d}^H]$. Ultimately, the lower bound of the average sum-rate can be derived from

$$R_{\text{sum}} = \frac{1}{S}\mathbb{E}_{\widehat{\mathbf{H}}}\left[\sum_{k=1}^{K}\sum_{l \in \mathcal{S}_u}\log_2(1 + SINDR_{k,l}(\widehat{\mathbf{H}}))\right]. \quad (19)$$

B. The Computation of $\mathbf{C}_{\mathbf{d}}$

To derive $\mathbf{C}_{\mathbf{d}}$, the vectorized forms of $\mathbf{d}_n^{(1)}$ and $\mathbf{d}_n^{(2)}$ over N time samples can be respectively expressed as

$$\mathbf{d}^{(1)} \triangleq j\mathbf{z} \odot \mathbf{e}_{\mathbf{\Psi}} + (\mathbf{e}_{\mathbf{A}} + j\mathbf{e}_{\mathbf{A}} \odot \mathbf{e}_{\mathbf{\Psi}}) \odot \exp(j\mathbf{\Psi}), \quad (20a)$$

$$\mathbf{d}^{(2)} \triangleq -\frac{1}{2}[\mathbf{z} + \mathbf{e}_{\mathbf{A}} \odot \exp(j\mathbf{\Psi})] \odot \mathbf{e}_{\mathbf{\Psi}}^2. \quad (20b)$$

Then, after some multiplication and addition operations of linear algebra, $\mathbf{C}_{\mathbf{d}}$ can be written as

$$\begin{aligned}\mathbf{C}_{\mathbf{d}} = \mathbf{C}_{\mathbf{e_A}} + (\mathbf{C}_{\mathbf{z}} + \mathbf{C}_{\mathbf{e_A}} + \mathbf{C}_{\mathbf{Ae_A}} + \mathbf{C}_{\mathbf{Ae_A}}^T) \odot \mathbf{C}_{\mathbf{e_\Psi}} \\ - \frac{1}{2}(2\mathbf{C}_{\mathbf{e_A}} + \mathbf{C}_{\mathbf{Ae_A}} + \mathbf{C}_{\mathbf{Ae_A}}^T) \odot \mathbf{C}_{\mathbf{e_\Psi}} \\ + \frac{1}{4}(\mathbf{C}_{\mathbf{z}} + \mathbf{C}_{\mathbf{Ae_A}} + \mathbf{C}_{\mathbf{Ae_A}}^T + \mathbf{C}_{\mathbf{e_A}}) \odot \mathbf{C}_{\mathbf{e_\Psi}}^2, \end{aligned} \quad (21)$$

where $\mathbf{C}_{\mathbf{z}} = (\mathbf{W}_N^H \otimes \mathbf{I}_{N_t})\widehat{\mathbf{P}}\widehat{\mathbf{P}}^H(\mathbf{W}_N \otimes \mathbf{I}_{N_t})$ denotes the covariance matrix of the transmitted signal $\mathbf{z}$ with Gaussian

This article has been accepted for publication in a future issue of this journal, but has not been fully edited. Content may change prior to final publication. Citation information: DOI 10.1109/LWC.2020.3046952, IEEE Wireless Communications Letters

signaling, $\mathbf{C}_{\mathbf{e_A}} = \mathbb{E}[\mathbf{e_A}\mathbf{e_A}^T] \in \mathbb{R}^{N_tN\times N_tN}$ and $\mathbf{C}_{\mathbf{e_\Psi}} = \mathbb{E}[\mathbf{e_\Psi}\mathbf{e_\Psi}^T] \in \mathbb{R}^{N_tN\times N_tN}$, respectively, denote the autocorrelation matrices for amplitude and phase quantization errors, and $\mathbf{C}_{\mathbf{Ae_A}} = \mathbb{E}[\mathbf{A}\mathbf{e_A}^T] \in \mathbb{R}^{N_tN\times N_tN}$. Furthermore, we have

$$\mathbf{C}_{\mathbf{A}^Q} = \mathbf{C}_{\mathbf{A}} + \mathbf{C}_{\mathbf{Ae_A}} + \mathbf{C}_{\mathbf{Ae_A}}^T + \mathbf{C}_{\mathbf{e_A}}, \tag{22}$$

where $\mathbf{C}_{\mathbf{A}^Q} = \mathbb{E}[\mathbf{A}^Q(\mathbf{A}^Q)^T] \in \mathbb{R}^{N_tN\times N_tN}$ is the autocorrelation matrix of amplitude output $\mathbf{A}^Q$.

Using (21) and (22), the derivation of $\mathbf{C_d}$ is given by

$$\mathbf{C_d} = \mathbf{C_{e_A}} + [(\mathbf{C_z} + \frac{1}{2}(\mathbf{C}_{\mathbf{A}^Q} - \mathbf{C_A} - \mathbf{C_{e_A}})] \odot \mathbf{C_{e_\Psi}} + \frac{1}{4}(\mathbf{C_z} + \mathbf{C}_{\mathbf{A}^Q} - \mathbf{C_A}) \odot \mathbf{C}^2_{\mathbf{e_\Psi}}. \tag{23}$$

C. Diagonal Approximation

For tractable analysis, a simple but accurate diagonal approximation method is utilized, where the quantization distortion is modeled as a white process, both in space and time, by assuming that the off-diagonal elements of $\mathbf{C_d}$ are zeros [5], [13]. Thus, the diagonal approximation $\mathbf{C}_{\mathbf{d}}^{\text{diag}}$ of $\mathbf{C_d}$ can be expressed as

$$\mathbf{C}_{\mathbf{d}}^{\text{diag}} = \mathbf{C}_{\mathbf{e_A}}^{\text{diag}} + [(\mathbf{C}_{\mathbf{z}}^{\text{diag}} + \frac{1}{2}(\mathbf{C}_{\mathbf{A}^Q}^{\text{diag}} - \mathbf{C}_{\mathbf{A}}^{\text{diag}} - \mathbf{C}_{\mathbf{e_A}}^{\text{diag}})] \odot \mathbf{C}_{\mathbf{e_\Psi}}^{\text{diag}} + \frac{1}{4}(\mathbf{C}_{\mathbf{z}}^{\text{diag}} + \mathbf{C}_{\mathbf{A}^Q}^{\text{diag}} - \mathbf{C}_{\mathbf{A}}^{\text{diag}}) \odot (\mathbf{C}_{\mathbf{e_\Psi}}^{\text{diag}})^2. \tag{24}$$

Let $a_m = [\mathbf{A}]_m$ be the m-th component of the amplitude input $\mathbf{A}$. Assume that the granular distortion is uniformly distributed, then its variance increases with increasing $\mathcal{A}_{\text{clip}}$ and is given by $\sigma^2_{g,m} = \frac{\mathcal{A}^2_{\text{clip}}}{12L_A^2}$. The overload distortion variance is given by

$$\begin{aligned}\sigma^2_{o,m} &= \int_{\mathcal{A}_{\text{clip}}}^{\infty} \frac{a}{\sigma_m^2}(a - a_{max})^2 \exp(-\frac{a^2}{2\sigma_m^2})da \\ &= \int_{\mathcal{A}_{\text{clip}}}^{\infty} \frac{a}{\sigma_m^2}\Big(a - \mathcal{A}_{\text{clip}}(1 - \frac{1}{2L_A})\Big)^2 \exp(-\frac{a^2}{2\sigma_m^2})da \\ &= \Big(2\sigma_m^2 + \frac{\mathcal{A}^2_{\text{clip}}}{4L_A^2}\Big)\exp(-\frac{\mathcal{A}^2_{\text{clip}}}{2\sigma_m^2}) - \frac{(2L_A-1)\mathcal{A}_{\text{clip}}}{L_A} \\ &\quad \times \sqrt{2\pi}\sigma_m Q(\frac{\mathcal{A}_{\text{clip}}}{\sigma_m}),\end{aligned} \tag{25}$$

where a_{max} denotes the maximum quantization output of the amplitude quantizer, $Q(x) \overset{def}{=} \frac{1}{\sqrt{2\pi}}\int_x^\infty \exp(-\frac{v^2}{2})dv$, and $\sigma_m^2 = \frac{1}{2}[\mathbf{C_z}]_{m,m}$. Then, the total distortion is the sum of $\sigma^2_{g,m}$ and $\sigma^2_{o,m}$ on the m-th entry of main diagonal of $\mathbf{C}_{\mathbf{e_A}}^{\text{diag}}$ [14].

Next, let a_m^Q be the m-th element of $\mathbf{A}^Q$. Then, the m-th element of the main diagonal of $\mathbf{C}_{\mathbf{A}^Q}^{\text{diag}}$ is given by

$$\mathbb{E}[|a_m^Q|^2] = \sum_{i=0}^{L_A-1} \ell_i^2 \mathbb{P}[\tau_i \le a_m \le \tau_{i+1}] \tag{26a}$$

$$= \sum_{i=0}^{L_A-1} \ell_i^2 \int_{\tau_i}^{\tau_{i+1}} \frac{v}{\sigma_m^2}\exp(-\frac{v^2}{2\sigma_m^2})dv \tag{26b}$$

$$= \sum_{i=0}^{L_A-1} \ell_i^2 \left(\exp(-\frac{\tau_i^2}{2\sigma_m^2}) - \exp(-\frac{\tau_{i+1}^2}{2\sigma_m^2})\right), \tag{26c}$$

where $\tau_i = i\frac{\mathcal{A}_{\text{clip}}}{L_A}, i = 0, \cdots, L_A$ and $\ell_i = \frac{(i+\frac{1}{2})\mathcal{A}_{\text{clip}}}{L_A}, i = 0, \cdots, L_A - 1$ are the quantization thresholds and labels of the amplitude quantizer, respectively. Finally, $\mathbf{C}_{\mathbf{z}}^{\text{diag}} = \text{diag}(\mathbf{C_z})$, the elements of main diagonal of $\mathbf{C}_{\mathbf{A}}^{\text{diag}}$ and $\mathbf{C}_{\mathbf{e_\Psi}}^{\text{diag}}$ are $(2 - 0.5\pi)\sigma_m^2, m = 1, \cdots, N_tN$ and $\frac{\pi^2}{3L_P^2}$, respectively. Note that $\mathbf{C}_{\mathbf{d}}^{\text{diag}} = \mathbf{C_d} \odot \mathbf{I}_{NtN}$ [13], which implies that the elements on the diagonal of $\mathbf{C_d}$ in (24) are exact.

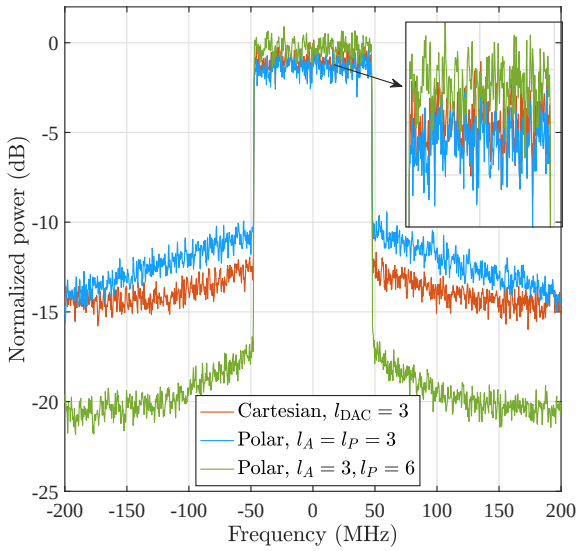

Fig. 2. PSD of the transmitted signal at the BS.

IV. Simulation Results and Conclusions

In the simulations, we consider a scenario that has $N_{cl} = 3$ clusters with uniformly distributed AoAs/AoDs in $[0, 2\pi)$. Each cluster consists of $N_{ray} = 2$ rays with Laplacian distributed AoAs/AoDs, and angle spread of 10° on each path. We also assume that there always exists a LOS path with the Ricean K-factor of 10 dB. Suppose that the maximum time delay spread is 60 ns. The chosen 100 MHz 64-QAM OFDM baseband signal is in line with 5G NR specifications [15] with subcarrier spacing of 60 kHz. There are $S = 1584$ active subcarriers with the normal cyclic prefix length, and the IDFT size is $N = 5 \times 2048$. Time-domain windowing is adopted to improve the spectral containment of the OFDM signals.

We consider a BS equipped with $N_t = 128$ antennas (half-wavelength spacing) and $K = 16$ UEs. We set $\mathcal{A}_{\text{clip}} = 1$ and set the average clipping probability of the amplitude signals to 10^{-2}. Then, the total transmit power is set to $P_{\text{total}} = N_t/(-\ln(10^{-2}))$ such that the I/Q signal on each antenna is $z_b \sim \mathcal{CN}(0, P_{\text{total}}/N_t), b = 1, \cdots, N_t$. We also plot the results of the Cartesian architecture with l_{DAC}-bit DACs for comparison, where $\mathcal{A}_{\text{clip}} = \frac{\sqrt{2}}{2}$ for the I/Q signals [5]. The results are the average over 100 channel realizations.

Fig. 2 shows the normalized power spectral density (PSD) of the transmitted signal, averaged over the antennas. We can see that higher phase resolution (e.g., 6-bit) can be used in the polar transmitter to reduce OOB emissions. Moreover, higher in-band power is emitted by using polar transmitter with higher number of phase bits.

In Fig. 3, the achievable average sum-rates versus quantization bits at different SNRs are presented. Fig. 3a shows that the average sum-rate of the unquantized polar transmitter can be approached by using very few amplitude bits and

This article has been accepted for publication in a future issue of this journal, but has not been fully edited. Content may change prior to final publication. Citation information: DOI 10.1109/LWC.2020.3046952, IEEE Wireless Communications Letters

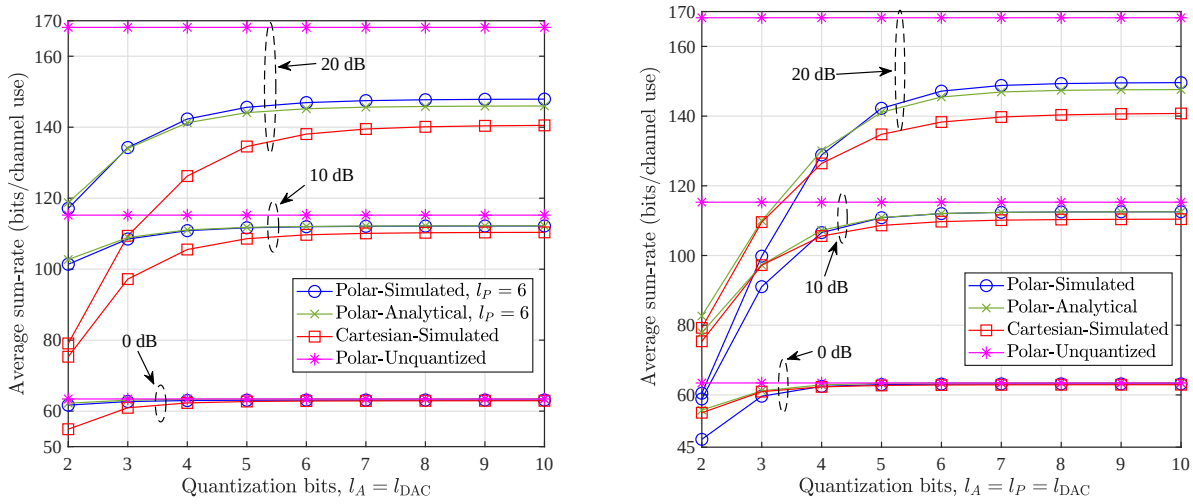

Fig. 3. Average sum-rate of polar architecture with ZF and 64-QAM under different amplitude and phase resolutions.

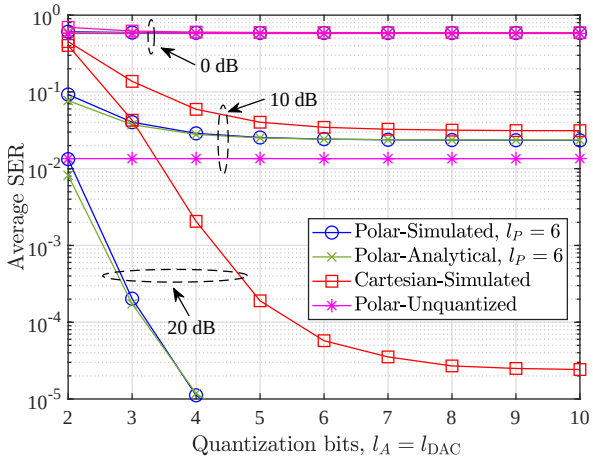

Fig. 4. Average uncoded SER performance of polar architecture for 64-QAM.

a moderate number of phase bits at the low and middle SNRs. For example, the performance loss is very small when l_A = 3-4 amplitude bits and l_P = 6 phase bits are employed at the SNR of 10 dB. However, the performance loss is becoming greater due to the quantization noise becoming dominant for SNR = 20 dB case. Moreover, good average sum-rate performance can be attained with 6-bit phase resolution and less amplitude resolution, i.e., 2-4 bits, compared to the Cartesian one with high-resolution DACs. Besides, it can be observed from Fig. 3b that the performance of the polar transmitter outperforms the Cartesian one with more than 4-bit quantization at the middle-high SNRs. Note that, the proposed diagonal approximation attains good accuracy for the case of $l_P \geq 4$ phase bits. Compared to Cartesian structure, the superiority of uncoded SER performance of polar transmitter is demonstrated in Fig. 4. As expected, the SER performance is significantly improved by increasing the amplitude resolution for $l_P = 6$ in the polar transmitter at SNRs of 10 dB and 20 dB. Additionally, only a few amplitude bits are required to approach the approximated SER performance, which again outperforms the Cartesian one.

These results, combined with the superior power efficiency of the polar architecture, make it highly appealing for future massive MIMO systems, and thus further studies on system performance and energy efficiency are warranted.

REFERENCES

[1] C. Fager *et al.*, "Linearity and efficiency in 5G transmitters: New techniques for analyzing efficiency, linearity, and linearization in a 5G active antenna transmitter context," *IEEE Microw. Mag.*, vol. 20, pp. 35–49, Apr. 2019.

[2] S. K. Mohammed and E. G. Larsson, "Per-antenna constant envelope precoding for large multi-user MIMO systems," *IEEE Trans. Commun.*, vol. 61, no. 3, pp. 1059–1071, Mar. 2013.

[3] H. Jedda, A. Mezghani, A. L. Swindlehurst, and J. A. Nossek, "Quantized constant envelope precoding with PSK and QAM signaling," *IEEE Trans. Wireless Commun.*, vol. 17, no. 12, pp. 8022–8034, Dec. 2018.

[4] M. Gümüş and T. M. Duman, "Multi-envelope precoding for massive MIMO systems," *IEEE Wireless Commun. Lett.*, vol. 7, no. 5, pp. 720–723, Oct. 2018.

[5] S. Jacobsson, G. Durisi, M. Coldrey, and C. Studer, "Linear precoding with low-resolution DACs for massive MU-MIMO-OFDM downlink," *IEEE Trans. Wireless Commun.*, vol. 18, pp. 1595–1609, Mar. 2019.

[6] J. Groe, "Polar transmitters for wireless communications," *IEEE Commun. Mag.*, vol. 45, no. 9, pp. 58–63, Sep. 2007.

[7] L. Ye, J. Chen, L. Kong, E. Alon, and A. M. Niknejad, "Design considerations for a direct digitally modulated WLAN transmitter with integrated phase path and dynamic impedance modulation," *IEEE J. Solid-State Circuits*, vol. 48, no. 12, pp. 3160–3177, Dec. 2013.

[8] K. Khalaf *et al.*, "Digitally modulated CMOS polar transmitters for highly-efficient mm-wave wireless communication," *IEEE J. Solid-State Circuits*, vol. 51, no. 7, pp. 1579–1592, Jul. 2016.

[9] C. Preissl, P. Preyler, T. Mayer, A. Springer, and M. Huemer, "Analysis of spectral degradation and error compensation in 5G NR digital polar transmitters," *IEEE Trans. Circuits Syst. I, Reg. Papers*, vol. 67, no. 8, pp. 2719–2729, Aug. 2020.

[10] P. Nazari *et al.*, "Polar quantizer for wireless receivers: Theory, analysis, and CMOS implementation," *IEEE Trans. Circuits Syst. I, Reg. Papers*, vol. 61, no. 3, pp. 877–887, Nov. 2014.

[11] R. B. Staszewski, "State-of-the-art and future directions of high-performance all-digital frequency synthesis in nanometer CMOS," *IEEE Trans. Circuits Syst. I, Reg. Papers*, vol. 58, pp. 1497–1510, Jul. 2011.

[12] 3GPP Tech. Rep. 38.901, "Study on channel model for frequencies from 0.5 to 100 GHz," *v15.0.0, (Release 15)*, Jun. 2018.

[13] E. Björnson, L. Sanguinetti, and J. Hoydis, "Can hardware distortion correlation be neglected when analyzing uplink SE in massive MIMO?" in *Proc. IEEE SPAWC*, Kalamata, Greece, Jun. 25-28, 2018, pp. 1–5.

[14] N. Al-Dhahir and J. M. Cioffi, "On the uniform ADC bit precision and clip level computation for a Gaussian signal," *IEEE Trans. Signal Process.*, vol. 44, no. 2, pp. 434–438, Feb. 1996.

[15] 3GPP Tech. Spec. 38.104, "NR; base station (BS) radio transmission reception," *v15.4.0, (Release 15)*, Dec. 2018.